Post-Launch Calibration of the TRMM Microwave Imager

Frank J. Wentz, Peter Ashcroft, and Chelle Gentemann

***Abstract*—Three post-launch calibration methods are used to examine the Tropical Rainfall Measuring Mission (TRMM) microwave imager (TMI) on-orbit performance. The first method is a statistical analysis of TMI ocean observations that reveals a systematic along-scan error. The second method is an intercomparison of TMI and SSM/I observations that shows a warm bias in TMI. The last method is an analysis of TMI observations taken during TRMMs deep-space maneuver. These deep-space observations confirm both the along-scan error found from method 1 and the warm bias found from method 2. The along-scan error exhibits distinctive features having amplitudes near 1 K. The warm bias, which is related to the scene temperature, can be as large are 5 K for ocean measurements. The physical explanation of a slightly emissive main reflector is proposed to explain the calibration errors.**

I. Introduction

THE TROPICAL Rainfall Measuring Mission (TRMM) spacecraft was launched In November 1997 [1]. One of the primary sensors flying on TRMM is the TRMM microwave imager (TMI), operating at frequencies between 10.7 to 85 GHz. TRMMs primary mission is to measure rainfall in the tropics. However, the inclusion of the new 10.7 GHz channel on TMI provides the additional capability to accurately measure sea-surface temperature (SST) through clouds [2]. Since the retrieval of SST requires precise radiometric calibration, we initiated a careful post-launch calibration of TMI shortly after launch. This paper describes the results of that calibration activity.

II. Sensor Description

Since the focus of TRMM is to measure rainfall in the tropics, a low inclination orbit was selected with the satellite subtrack confined from 35°S to 35°N. Also, a relatively low altitude of 350 km was chosen to provide better spatial resolution. The orbit is not sun-synchronous, and the local time at the ascending node time precesses 24 h every 46 days.

TMI consists of nine separate total-power radiometers, each simultaneously measuring the microwave emission coming from the Earth and intervening atmosphere. The nine channels correspond to four dual polarization frequencies (10.7, 19, 37, 85 GHz) and one single polarization (v-pol) channel at 21.3 GHz. TMI uses an offset parabolic reflector to collect the microwave radiation. The reflector focuses the radiation into two feedhorns (one for 10.7 GHz and the other for 19–85 GHz). The reflector and feedhorns spin as a unit about an axis parallel to the spacecraft nadir. The rotation period is 1.9 s. A cold-space mirror and a warm reference load are attached to the spin axis and do not rotate. The rotating feedhorns observe the fixed cold mirror and warm load once each scan. In this way, calibration observations are taken every scan.

Earth observations are taken during a 130° segment of the rotation. The 130° arc is centered on the spacecraft subtrack and maps out a 760 km swath on the Earth's surface. The 760 km swath and the low inclination angle provide coverage from 39°S to 39°N. During each scan, the 10.7–37 GHz observations are sampled 104 times over the 130° arc. The 85-GHz observations are at a higher spatial resolution and are sampled twice as frequently (208 observations/scan).

III. Calibration Methods

This analysis employed three calibration techniques. The first is a statistical regression method used to find systematic errors related to scan position. This method only requires TMI ocean observations. The second method is an intercomparison between the TMI observations and collocated observations taken by the special sensor microwave imager (SSM/I). The third method is an analysis of the TMI observations during an orbit maneuver in which the TMI main reflector observed cold space (2.7 K). For all three methods, the TMI observations are expressed in terms of the antenna temperature T_A. Each of these methods is now discussed.

A. Statistical Analysis of Ocean Observations

TMI is a conically scanning radiometer, maintaining a nearly constant Earth incidence angle throughout the scan. In principle, the measurement characteristics of the sensor should be completely independent of scan position. However, in practice, problems such as spacecraft attitude errors, obstructions in field of view, and sidelobes seeing the spacecraft may result in systematic errors that are a function of scan position. Given enough observations, we might determine the along-scan error by making the assumption that the effect of weather and surface features will, on the average, be the same at all scan positions. If this is the case, then the along-scan error can be detected simply by binning the TMI observations according to the 104 scan positions and then averaging for several months. If the resulting curves are not flat when plotted versus scan position, then this is an indicator of systematic errors.

Unfortunately, the average effect of weather and surface features is not the same for all scan positions. Two examples of complicating factors are the systematic geographic effects of

Manuscript received January 26, 2000; revised May 30, 2000. This work was supported by the NASA TRMM Science Team, Washington DC, Contract NAS5-99191.

The authors are with Remote Sensing Systems, Santa Rosa, CA 95401 (e-mail: wentz@remss.com).

Publisher Item Identifier S 0196-2892(01)01166-4.

latitudinal SST and water vapor variation. Because TRMM is in a low inclination orbit, the scan geometry has an appreciable north–south component. If not accounted for, real latitudinal variations in the geophysical parameters can be misinterpreted as an along-scan error. Consequently, a linear regression technique is used to decouple geographical effects from scan position effects. A geographical index i is defined that points to 1°-latitude by 1°-longitude cells on the ocean surface. The T_A observations at geographical location i and scan position j are expressed by

$$T_A(i, j) = \hat{G}(i) + \hat{B}(j) + \varepsilon \tag{1}$$

where the elements of vector $\hat{G}$ are some constant T_A value for each 1° cell, and the vector$\hat{B}$ is the desired along-scan error. The term ε is the residual error on each observation. The scan index j ranges from 1 to 104 (1 to 208 for 85 GHz). The geographic effects are further diminished by using only observations within a restricted latitudinal band of 30°S to 30°N, for which the north-south component of the scan is not too large. A simple rain flag is also used to further filter the data. There are approximately 14 000 1°-cells in the ocean between 30°S to 30°N. Hence, i ranges from 1 to about 14 000. The vectors $\hat{G}$ and $\hat{B}$ are found so as to minimize the sum of the squared residual errors ε, (inversely weighted by their variance) and subject to the constraint that $\sum \hat{B}(j) = 0$. This requires solution of approximately $(14\,000 + 104 + 1)$ simultaneous linear equations with the same number of unknown parameters.

TRMMs yaw orientation is reversed at approximately monthly intervals to compensate for the satellite's diurnal drift through the solar day. In this way, the spacecraft components are protected from excessive solar heating. For our analysis, we divide the year 1998 into six two-month periods, and observations within each two-month period are binned according to one of the two yaw orientations (0° and 180°). This gives six groups for each yaw. A separate along-scan error $\hat{B}$ is found for each group. One effect of the yaw maneuver is that the latitudinal relationship of the observations reverses. In other words, the first scan position generally samples more northerly locations than the final scan position for one yaw orientation, but the geometry is reversed when the yaw orientation changes. The geographical decomposition in (1) helps eliminates these and other sampling effects.

B. Comparison of TMI with SSM/I

SSM/I is an operational microwave radiometer that flies aboard the Defense Meteorological Satellite Program (DMSP) spacecraft [3]. During the time of this analysis, three SSM/Is were in operation: F10, F11, and F13. SSM/I has proven to be a very stable sensor, and its absolute calibration as compared to radiative transfer models is estimated to be between 1 and 2 K [4]. Thus, it can be used as a calibration source for TMI except for the 10.7 GHz channels which are missing from SSMI.

The TMI instrument is similar to SSM/I, with some notable exceptions. TMI has an additional feedhorn to accommodate the 10.7 GHz channel, and the frequency of the water vapor channel for TMI is 21.3 GHz as compared to 22.235 for SSM/I. TMI also has a wider active scan (130° versus 102° for SSM/I), and the fabrication of TMIs main reflector is slightly different (see below). In addition, TRMMs altitude is much lower than the DMSP spacecrafts (350 versus 830 km), and to maintain an Earth incidence angle near 53°, the nadir cone angle for TMI is 49° as compared to 45° for SSM/I. The actual incidence angle for TMI is 52.75° ± 0.1° as compared to 53.4° ± 0.3° for SSM/I.

A standard radiative transfer model [5] is used to normalize the SSM/I T_As to a constant incidence angle of 52.75° (the TMI value) and to convert the 22.235 GHz observations to a frequency of 21.3 GHz (the TMI value). Over the ocean, the magnitude of the incidence angle adjustment is about 1 K, while the frequency adjustment can be as large as 10 K. These adjustments are not constant but depend on the atmospheric transmittance, which is inferred from the observations. No adjustment is made to land observations because 1) the incidence angle and frequency dependence of T_A is small, and 2) we do not have reliable models for the incidence angle and frequency variation of land observations.

Having adjusted the SSM/I T_A to correspond to TMI, daily T_A maps (one for the ascending orbit segment and another for the descending orbit) are made at a latitude-longitude pixel resolution of 1.0°. For each TMI observation, the SSM/I maps are searched to find the closest pixel within a 0.7° spatial window and a 30-min time window. If no SSM/I pixel is found within the prescribed window, then no TMI-SSM/I collocation is recorded. The results of the TMI-SSM/I collocation are summarized in terms of a two-dimensional (2-D) joint probability density function (JPDF), where the two dimensions are the TMI minus SSM/I T_A difference and the SSM/I T_A. The analysis uses all three operational SSM/Is (F10, F11, and F13) for the time period from December 1997 through April 1998.

C. Deep-Space Observations

As part of the Clouds and the Earths Radiant Energy System (CERES) calibration process, the TRMM platform was pitched to view deep space rather than the Earth during several orbits in January 1998 and again in September 1998. Although not intended for the benefit of the TMI instrument, these maneuvers proved to be extremely useful for calibrating TMI and for confirming the other two calibration methods. When the spacecraft is pitched 180° relative to the Earth nadir, the TMI main reflector has a clear view of deep space that is at a nearly uniform temperature of 2.7 K. Given a homogenous scene at a known temperature, calibration errors are readily detectable. As we will show, the results obtained from the deep space observations are remarkably consistent with those coming from the more elaborate analyses involving Earth observations.

IV. Results

The first two calibration methods detected two types of calibration errors: 1) a small ($\leq$1 K) systematic error that is correlated with the scan position, and 2) a warm bias in the TMI T_A that is related to the temperature of the scene being viewed by the main reflector.

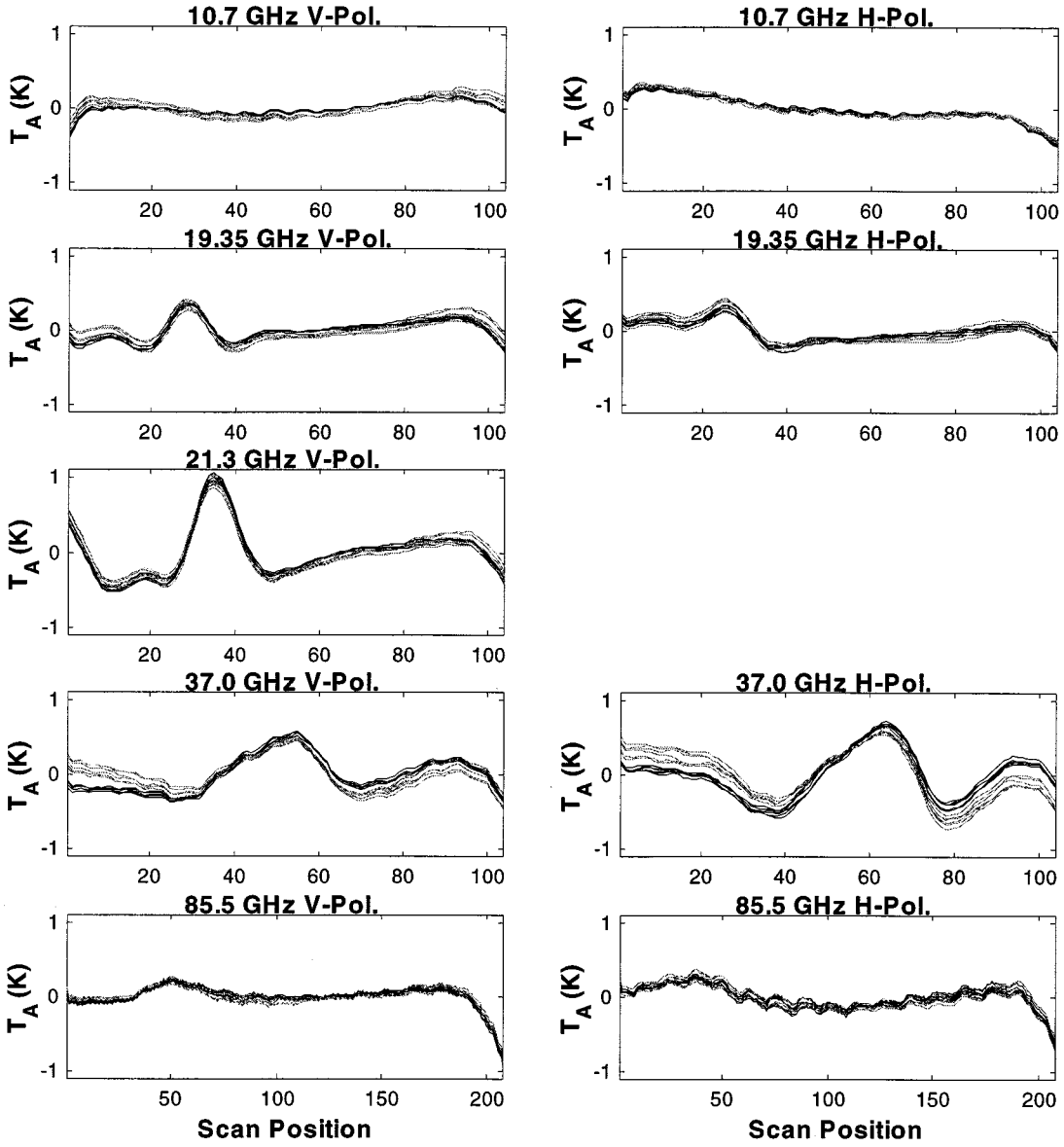

Fig. 1. Along-scan error for six monthly time periods and two yaw orientations in 1998. The observed T_A anomaly is plotted versus scan position. The gray (black) curves are for a yaw of 180° (0°).

A. Along-Scan Error

The along-scan error is determined from two completely independent methods: monthly averages of ocean observations and the analysis of the deep-space observations. Fig. 1 shows the results for the ocean observations for the entire year of 1998. The 1999 ocean results are almost identical. Each of the along-scan error curves shown in this figure is constrained to have a sum over all scan positions of zero. The ocean observations are partitioned according to a two-month time period and yaw orientation, giving six curves for each of the two yaws (0° or 180°). The curves clearly show the existence of a distinct along-scan error for each frequency. For a given channel, the 12 curves for the various time periods and yaws show remarkable consistency except at 37 GHz, where the two yaw orientations display a small difference. It is not clear why the yaw orientation would only affect the 37 GHz channels, nor is it clear why there would be more variation among time periods for the 37 GHz channels. We investigated the possibility that systematic wind direction or incidence angle effects might account for the difference between the two yaws, but we concluded that neither of those effects could explain the difference. In any event, the yaw discrepancy at 37 GHz is small compared to the observed along-scan error, and the other channels show a high degree of consistency among the six time periods and two yaws, which tends to validate the reliability of the ocean calibration method.

The deep-space observations yield similar along-scan errors. Fig. 2 shows the results coming from the first deep-space maneuver (January 1998) overlaid by the averaged 1998 ocean results. The along-scan errors for the second maneuver (September 1998, not shown) are similar, but with a coincidental appearance of the moon in the middle of the

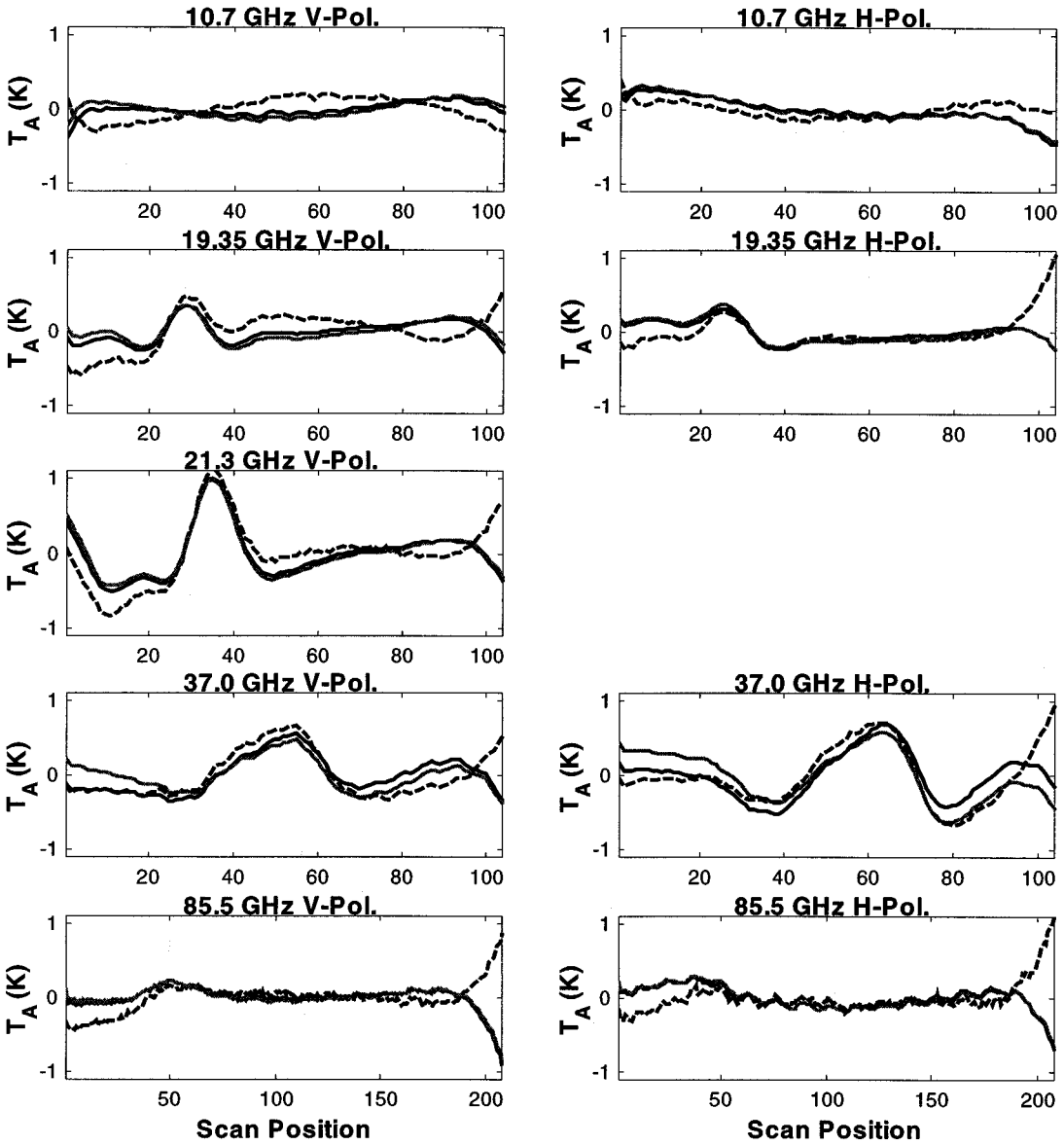

Fig. 2. Comparison of the average along-scan error derived from ocean observations and from deep-space observations. The observed T_A anomaly is plotted versus scan position. The solid black and gray curves come from ocean observations for yaw orientations of 0° and 180°, respectively, during 1998. The dashed curves come from deep-space observations during January 1998.

scan. Approximately 300 scans are averaged to produce the along-scan error for these deep-space observations as compared to the millions of scans required for the ocean analysis.

The ocean and deep-space observations show the same lobe-shaped features in the middle of the scan. In addition, they both reveal smaller features that are remarkable for their lockstep consistency, such as the fine saw-tooth structure in the 85 GHz channels. The similar magnitude of the bias of the ocean and deep-space observations indicates that the along-scan error in the middle of the scan is essentially independent of the actual scene temperature. This is significant because it makes correction very straightforward. The ocean observations are typically between 90 and 220 K, depending on channel, and the deep-space observations are at 2.7 K. However, at the end of the scan, there is a significant difference between the ocean and deep-space observations. The ocean observations generally show a downturn at the end of the scan while the deep-space observations show an upturn (except at 10.7 GHz). SSM/I ocean observations also show a downturn at the end of the scan, and it was supposed that some obstruction (either the cold mirror or some part of the spacecraft) was coming into the view of the SSM/I main reflector [3], [6]. This explanation applies equally well to the TMI. If the field-of- view obstruction has an apparent temperature colder than the ocean observations but warmer than 2.7 K, then this would explain both the downturn for ocean observations and the upturn in the deep-space observations. However, in other respects, the SSM/I and TMI along-scan results are quite different. For example, the SSM/I did not show any appreciable along-scan error in the middle of the scan. The mechanism producing the major along-scan features in the middle of

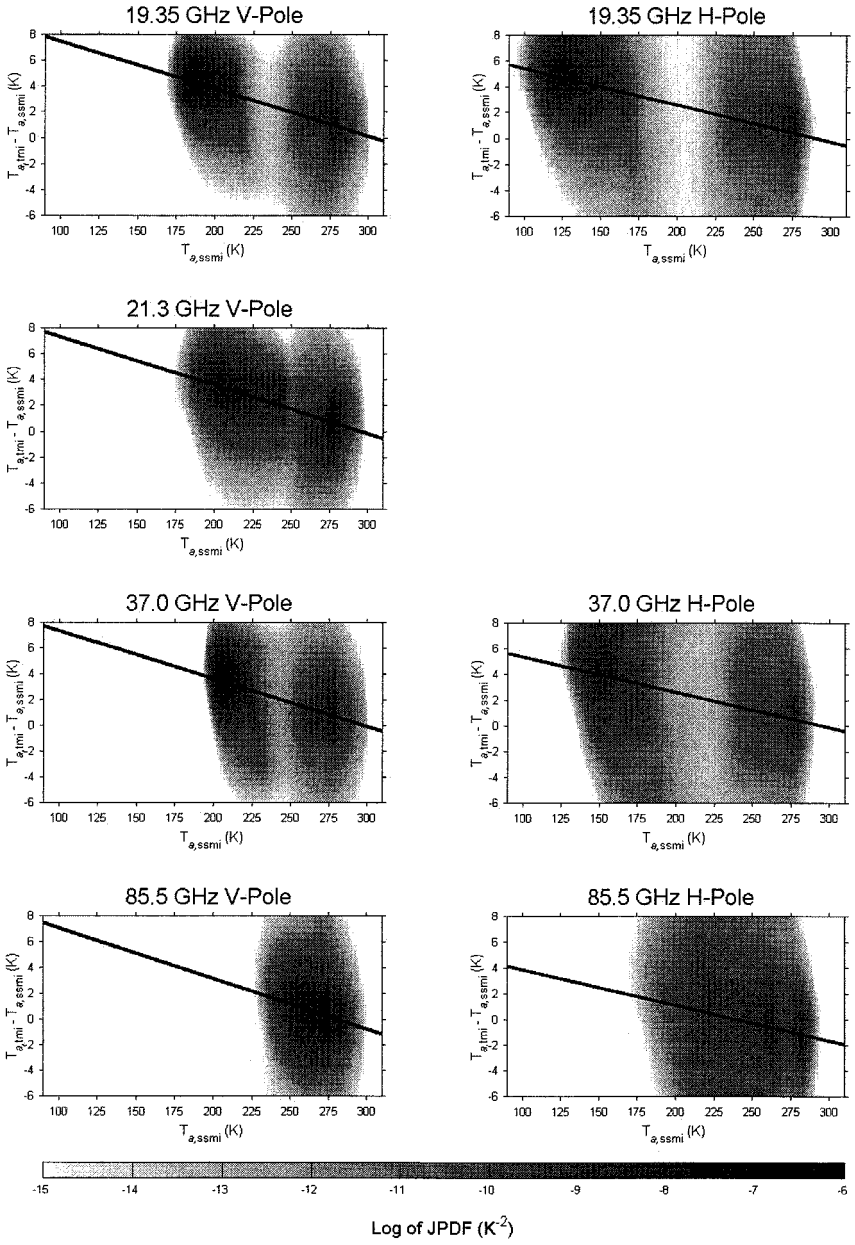

Fig. 3. Joint probability density function (JPDF) of the TMI minus SSM/I T_A difference versus the SSM/I T_A. The shaded background shows the logarithm of the JPDF, and the black line is the least-squares fit to the JPDF.

TABLE I
SLOPES AND INTERCEPTS OF LEAST SQUARES FIT FOR THE TMI VERSUS SSM/I T_A INTERCOMPARISON

Frequency	Slope, a		Intercept (K), b	
	V Pol.	H Pol.	V Pol.	H Pol.
19.3 GHz	-0.0370	-0.0284	11.2	8.2
21.3 GHz	-0.0377		11.1	
37.0 GHz	-0.0375	-0.0274	11.1	8.1
85.5 GHz	-0.0396	-0.0277	11.1	6.6

the TMI scan is not currently understood, nor is the source of the fine sawtooth structure in the 85-GHz channels. Nevertheless, the error is sufficiently consistent across a wide range of scene temperatures, (from cold space to ocean scenes), that a general correction can be applied.

B. Warm Bias

The comparison of the TMI and SSM/I antenna temperatures is given in Fig. 3, which shows the JPDF of $T_{A,\,\mathrm{TMI}} - T_{A,\,\mathrm{SSM/I}}$ versus $T_{A,\,\mathrm{SSM/I}}$ for seven of the nine TMI channels. No SSM/I comparisons are available for the two 10.7 GHz channels. For all channels except 85.5 GHz, the observations have a distinct bimodal distribution: warm land and cool ocean. The 85.5 GHz channel is more sensitive to the atmosphere and therefore does not delineate ocean/land measurements as clearly. The black line is the following linear least-squares fit to the data:

$$T_{A,\,\mathrm{TMI}} - T_{A,\,\mathrm{SSMI}} = aT_{A,\,\mathrm{SSMI}} + b. \tag{2}$$

The slope a and intercept b are given in Table I. The JPDF shows the variability of the observations about the least-squares fit.

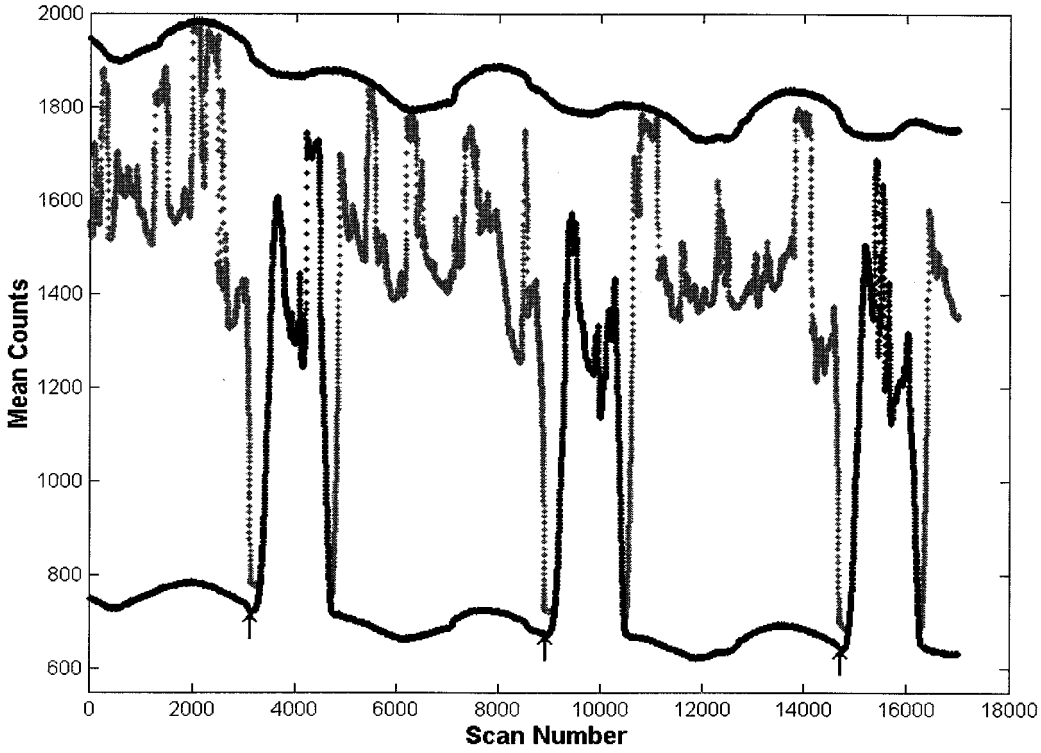

Fig. 4. Time series of radiometer counts for the hot-load (black), cold-mirror (black), and main-reflector (gray) during the deep-space maneuver in January 1998. Arrows show when the cold mirror and main reflector simultaneously viewed deep space.

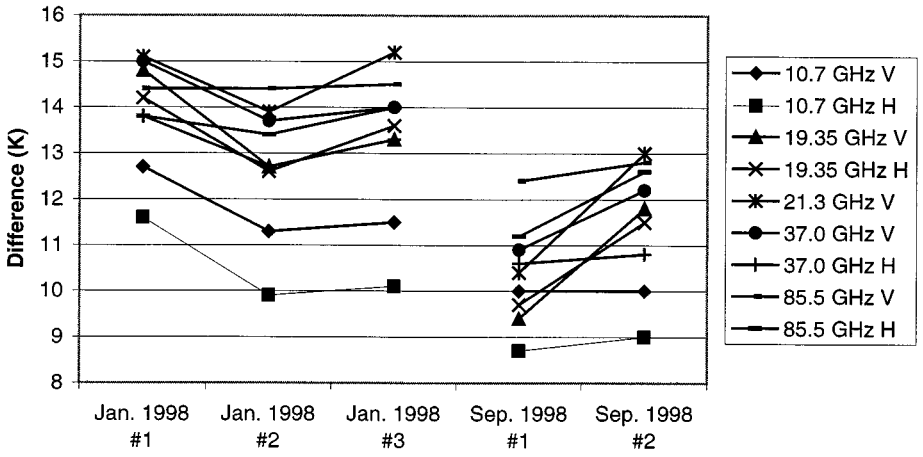

Fig. 5. Warm bias of the main reflector relative to the cold mirror for simultaneous observations of deep space. Three of these events occurred in January 1998 and then another two in September 1998.

The variance is mostly due to spatial/temporal differences (i.e., weather features) associated with the TMI-SSM/I collocation.

All seven channels show nearly the same characteristic. For very warm Earth scenes ($\approx$ 295 K), the TMI and SSM/I values are in close agreement, but as the scene temperature decreases, the TMI TA shows a warm bias relative to SSM/I. For cold ocean observations, the TMI-SSM/I offset reaches values as high as 5 K. A 5 K calibration error is very large. For example, the inter-satellite calibration offsets for the series of five SSM/Is are an order of magnitude smaller ($\approx$ 0.5 K) [3], [6].

The deep-space observations provide an independent assessment of the TMI warm bias. Extrapolating the TMI-SSM/I comparisons to a scene temperature of 2.7 K predicts a TMI warm bias near 10 K. If this result is correct, it should be easily discernable in the deep-space observations. Fig. 4 shows the variation of radiometer counts for 1) the warm load, 2) cold mirror counts, and 3) main reflector as TRMM performed its pitch maneuver and pointed toward deep space. The maneuver was done three times over a period of nine hours. Fig. 4 shows the results for the 19 GHz v-pol channel. Other channels show similar patterns. Each of the points in the figure represents a single TMI scan having 104 main reflector observations (208 for 85 GHz), eight cold-mirror observations and eight warm-load observations. At the start of the maneuver, the main reflector is viewing the Earth and the cold mirror sees deep space. As the spacecraft is pitched, the footprint of the main reflector moves toward the Earths limb and then views deep space. This transition is shown by a steep reduction in counts. Meanwhile, the cold mirror is

going through an opposite transition, going from deep space to viewing the Earth. During a brief period of time (∼100 scans), both the main reflector and the cold mirror have a clear view of deep space. When the cold mirror counts exceeded the main reflector counts, the TMI Level-1 algorithm interpreted this as an error condition, and the main reflector counts were reset to the default value of 0. As a result, the main reflector counts are not available during much of the deep space observation time. This artifact of early TMI processing was remedied for the second deep-space maneuver.)

The simultaneous viewing of deep space by the main reflector and the cold mirror confirms the warm bias in the TMI observations. Fig. 5 shows the results for five observations of deep space (in January 3, 1998 and in September 2, 1998). The antenna temperature for the main reflector is clearly higher than that for the cold mirror. The warm bias is between 9 and 15 K, depending on channel and specific observation. The variability in the results (±3 K) is somewhat larger than we had expected.

V. Possible Explanations for Calibration Errors

That portion of the along-scan error that occurs near the end of the scan is probably due to some obstruction in the field of view (either the cold mirror or some part of the spacecraft), as has already been discussed in Section IV-A. However, we have no obvious explanation for the lobe-like structures seen in the middle scan. These features are absent from SSM/I. The fact that the lobe-like structures are about the same magnitude for the ocean and deep-space observations suggests the possibly that an antenna sidelobe or backlobe (i.e., spillover) is sweeping from cold space, across the warmer spacecraft, and then back again to cold space. Interference from the precipitation radar (PR), (an active instrument on the TRMM platform), was considered as another explanation. Temporarily placing the PR in standby mode (nonradiating) for one minute during the second deep-space maneuver caused no change in the TMI measurements, thereby exonerating the PR.

The TMI warm bias has a very distinct characteristic in that it is well described as a linear function of scene temperature. This suggests that some unknown warm emitter is in the TMI field of view. A simple error model for this type of interference is

$$T_{A,\,\mathrm{TMI}} = (1-\varepsilon)T_A + \varepsilon T_0 \tag{3}$$

where

- $T_{A,\,\mathrm{TMI}}$ measurement;
- T_A true antenna temperature of the incoming radiation;
- T_0 and ε physical temperature and emissivity of the unknown emitter in the field of view (possibly the antenna itself).

Taking the SSM/I observations as an indicator of the true T_A, (2) and (3) can be combined to obtain the following relationships:

$$\varepsilon = -a \tag{4}$$

$$T_0 = \frac{-b}{a}. \tag{5}$$

TABLE II
Parameters Relating to the Model for the TMI Warm Bias. The Emissivity ε and Temperature T_0 of the Unknown Emitter are Given Along with the Predicted and Observed Warm Bias at $T_A = 2.7$ K

Channel	ε	T_0 (K)	$\Delta T_{A,\,\mathrm{pred}}$ (K)	$\Delta T_{A,\,\mathrm{obs}}$ (K)
19V	0.0370	302.3	11.1	12.4
19H	0.0284	290.4	8.2	12.3
21V	0.0377	294.6	11.0	13.5
37V	0.0375	296.1	11.0	13.2
37H	0.0274	294.7	8.0	12.2
85V	0.0396	279.6	11.0	13.7
85H	0.0277	239.6	6.6	13.0

Thus, one can use the SSM/I versus TMI comparison to estimate the temperature and emissivity of the hypothesized error source. As shown in Table II, the emissivity ε is between 3 and 4%, and its temperature is between 295 and 302 K, except at 85 GHz. The 85 GHz channels are very sensitive to atmospheric moisture (i.e., changing weather patterns) and exhibit a smaller overall range of T_A from ocean to land. Both these effects make it more difficult to separately estimate ε and T_0. This probably explains the discrepancy between the 85 GHz values and the values obtained for the lower frequency channels.

Given ε and T_0, (3) can then be used to predict $T_{A,\,\mathrm{TMI}}$ for the TRMM deep-space maneuver, for which $T_A = 2.7$. The predicted warm bias ($T_{A,\,\mathrm{TMI}}$ minus 2.7) is given in Table II under the column $\Delta T_{A,\,\mathrm{pred}}$, and the warm bias that was observed during the deep space maneuver is given in the last column ($\Delta T_{A,\,\mathrm{obs}}$). The values for $\Delta T_{A,\,\mathrm{obs}}$ in Table II come from averaging the five values shown in Fig. 5. The agreement between the predicted versus and observed warm bias for $T_A = 2.7$ is typical within about 3 K.

The error model is further supported by some recent results that show the warm bias is directly related to the physical temperature of the main reflector. Within a single orbit, the main reflector temperature is estimated to have a peak-to-peak variation of about 80 K due to direct solar heating and subsequent nighttime cooling. An analysis of day- versus-night T_A values reveals rather large discrepancies that cannot be explained by natural diurnal variations of the Earth. The day-night T_A differences are about 3 K. Dividing this by the corresponding temperature variation of the main reflector (80 K) gives 4%, which is generally consistent with the emissivity values given in Table II.

Equation (3) provides a good representation for the TMI warm bias. It accurately models: 1) the discrepancy in the TMI-SSM/I intercomparisons; 2) the offset between the main reflector and cold mirror during the deep-space maneuvers; and 3) the more recent results, which show the warm bias is correlated to the physical temperature of the main reflector.

After submitting this paper for publication, we received new information from the TMI vendor about the VDA coating. At the TRMM altitude of 350 km, there is an appreciable amount of atomic oxygen. The assumption before launch was that the atomic oxygen would produce a very thin protective layer of aluminum oxide on the VDA surface, and the remainder of the VDA would remain intact. However, after further consideration, prompted by the results presented herein, it appears that small pits in the VDA may have allowed the oxidation to penetrate through the VDA, undermining the adhesion of the VDA to the

underlying graphite antenna structure. It now seems likely that all of the VDA either oxidized or flaked off shortly after launch, leaving a bare graphite antenna. This conclusion is supported by the results presented here in that graphite has a spectrally flat reflectivity of the order of 96%.

VI. Conclusion

The TMI sensor has two significant calibration errors: an along-scan error and a warm bias that is related to the scene temperature. The along-scan error may be partially explained by a field-of-view obstruction (either the cold mirror or spacecraft) that occurs near the end of the scan. The warm bias is probably due to a slightly emissive antenna. Corrections need to be made to raw TMI antenna temperature measurements to compensate for these calibration errors. Version 5 of the TMI data products incorporates both the along-scan and warm bias corrections discussed in this paper. The along-scan correction is the mean of the corrections for each yaw orientation observed during the 1998 ocean observations, while the offset correction is derived from the rollover maneuver observation of cold space (very similar to the correction inferred from comparison to SSM/I).

The deep-space observations proved to be an extremely valuable calibration tool. We recommend that this type of maneuver be conducted for other microwave radiometer missions such as the advanced microwave scanning radiometers (AMSRs) that will fly on NASAs Aqua platform and on NASDAs ADEOS-2 platform. We also recommend that the emissivity of the main reflector be measured when fabricating future satellite radiometers. As an additional precaution, precision thermistors should be attached to the main reflector to allow for an emissivity correction after launch. Finally, we recommend that the calibration methods discussed here be routinely applied to AMSR and other future satellite microwave radiometers.

References

[1] C. Kummerow, W. Barnes, T. Kozu, J. Shiue, and J. Simpson, "The tropical rainfall measuring mission (TRMM) sensor package," *J. Atmos. Ocean. Technol.*, vol. 15, pp. 809–817, 1998.

[2] F. J. Wentz, C. Gentemann, D. Smith, and D. Chelton, "Satellite measurements of sea-surface temperature through clouds," *Science*, to be published.

[3] M. C. Colton and G. A. Poe, "Intersensor calibration of DMSP SSM/I's: F-8 to F-14, 1987–1997," *IEEE Trans. Geosci. Remote Sensing*, vol. 37, pp. 418–439, Jan. 1999.

[4] F. J. Wentz, "A well-calibrated ocean algorithm for SSM/I," *J. Geophy. Res.*, vol. 102, no. C4, pp. 8703–8718, 1997.

[5] ——, "Algorithm Theoretical Basis Document (ATBD): AMSR Ocean Algorithm," RSS Tech. Rep. 110 398, Remote Sensing Systems, Santa Rosa, CA, Nov. 1998.

[6] ——, "User's Manual SSMII Antenna Temperature Tapes, Revision 2," RSS Tech. Rep. 120 193, Remote Sensing Systems, Santa Rosa, CA, Dec. 1993.

Frank J. Wentz received the B.S. and M.S. degrees, both in physics, from the Massachusetts Institute of Technology, Cambridge, in 1969 and 1971, respectively.

In 1974, he established Remote Sensing Systems (RSS), Santa Rosa, CA, a research company specializing in satellite microwave remote sensing of the Earth. His research focuses on radiative transfer models that relate satellite observations to geophysical parameters, with the objective of providing reliable geophysical data sets to the earth science community. As a member of NASAs SeaSat Experiment from 1978 to 1982, he pioneered the development of physically-based retrieval methods for microwave scatterometers and radiometers. Starting in 1987, he took the lead in providing the worldwide ocean research community with high quality ocean products derived from satellite microwave imagers (SSM/I). He is currently a member of the NASA Earth Observation System (EOS) Investigators Working Group, NASA Advanced Microwave Scanning Radiometer (AMSR) Team, the NASA Tropical Rainfall Measuring Mission (TRMM), and NASA Pathfinder activity. He has served on many NASA review panels. He is currently working on satellite-derived decadal time series of atmospheric moisture and temperature, the measurement of sea-surface temperature through clouds, and advanced sensor designs for climatological studies.

Dr. Wentz is a member of the American Geophysical Union.

Peter Ashcroft received the B.S. in applied physics from the California Institute of Technology, Pasadena, in 1986, and the Ph.D. from the Department of Engineering and Public Policy, Carnegie Mellon University (CMU), Pittsburgh, PA, writing his doctoral dissertation on the relative merits of ground, air, and space-based methods for characterization of methane sources on the Earths surface.

From 1986 to 1988, he was with Lockheed Missiles and Space Corp., Sunnyvale, CA. He joined Remote Sensing Systems (RSS), Santa Rosa, CA, in November 1995. Since then, he has worked on spatial resampling of microwave radiometer observations (for the AMSR-E instrument), data and processing format issues for AMSR-E, and calibration of the TMI instrument.

Chelle Gentemann received the B.S. degree in earth, atmosphere, and planetary sciences from the Massachusetts Institute of Technology, Cambridge, in 1995, and the M.S. degree in physical oceanography from Scripps Institute of Oceanography, La Jolla, CA, in 1997.

Since 1997, she has been with Remote Sensing Systems (RSS), Santa Rosa, CA. Her research is focused on the cal/val effort for TMI and cal/val of the SST algorithm RSS has developed for TMI. She is also active in research of tropical instability waves and oceanic cold wakes of hurricanes.